High-Gain Magnetically Insulated Impact Fusion via Staged Explosive Acceleration to Hypervelocity

Finn van Donkelaar

University of Washington

MSAA ‘20

Contents

Introduction

This report describes the theoretical basis for and simplistically calculates the performance of a method for initiating high-gain thermonuclear reactions using chemical explosives. The proposed system would be compact and miniaturizable, but would have a lower yield-to-weight ratio than current thermonuclear devices. As in other thermonuclear devices, there is the potential for extensive optimization of the design due to the interplay between nuclear, kinetic, chemical and magnetic energy that occurs during detonation.

This system presents a significant challenge to nuclear non-proliferation efforts by eliminating the requirement for fissile primary stages in thermonuclear weapons. Furthermore, the manufacturing tolerances and engineering techniques required for its construction are commonplace at yields above 500 tons TNT equivalent.

1.0 Background

Three technologies are harnessed to produce fusion in this system. In order to understand the advantages of the third (staged explosive launchers) it is necessary to learn about the phenomenon of overdriven detonation in solid explosives.

1.1 Inertial Confinement Fusion

When a pellet of dense fusion fuel is imploded at high velocity, the inertia of the atoms composing the fuel will keep it intact for a period of time sufficient for high-gain fusion to occur. Confinement time is increased by surrounding the fuel in a “tamper” constructed out of heavy elements such as tungsten. ICF is the only form of fusion to have been successfully harnessed-in thermonuclear weapons, which use the energy produced by a “primary” nuclear fission stage to initiate fusion in a “secondary” fusion stage, as well as fission in a fissile tamper.

1.2 Magnetically Insulated Impact Fusion

MIIF uses inertial confinement, but the efficiency of the reaction is increased by introducing magnetic fields into the plasma. Sufficiently powerful fields will cause the alpha particles emitted by the D-T reaction to orbit within the plasma, reducing the energy loss caused by heat conduction to the tamper [1], [2]. The fields have an initially low intensity, but are intensified by the compression of the tamper.

1.3 Overdriven Detonation

The behavior of detonating high explosives is described by the Zel’dovich-Neumann-Doring (ZND) and Chapman-Jouguet (CJ) models. Both models specify an initial shock which propagates into the explosive, compressing and heating the material. In the ZND model, the explosive remains unreacted until the shock passes. At this point, exothermic chemical reactions occur. The shock is sustained by energy generated by these reactions. The energy generated by the reactions can be transmitted to the shock only because the high pressure of the reaction products ensures that the shock will be sonic from their reference frame. Thus, the shock is limited to the sonic velocity of the detonation products without some external energy input. The CJ model describes the resulting equilibrium detonation pressure, temperature and velocity of the detonation wave.

When an object strikes a solid explosive at sufficiently high velocity, it induces a shock of higher pressure and initial velocity than the CJ values. The detonation of the explosive then proceeds at a significantly faster rate because the shock propagates into the material without being solely sustained by the energy of the detonation products. Some energy is transmitted from the detonation products to the shock because the sonic velocity is increased by the shock pressure. However, overdriven detonation waves are not truly self-propagating and will degenerate to ordinary CJ detonation waves as they travel deeper into the explosive.

1.4 Staged Explosive Launchers

A single explosive charge is limited in the velocity that it can impart to a flyer plate by its detonation velocity and the pressure of its detonation products. With chemical explosives, this generally results in flyer velocities between 3-5 km/s. However, this limit can be circumvented by staging layers of explosives and flyers.

Staging allows previous stages to deposit kinetic energy into the next flyer, while simultaneously initiating overdriven detonation in the next explosive layer. The enhanced explosive properties caused by overdriven detonation, in combination with the densification of kinetic energy caused by staging, allow practical final flyer velocities between 8-12 km/s [3], [4].

2.0 Design Concept

The system is built around the MIIF design proposed by Ribe and Barnes in [2] combined with the gain-boosting concept which Winterberg describes in [1]. A staged explosive launcher is substituted for the original railgun to make the system self-contained and compact. For brevity, the two halves of the inertial confinement system are referred to as the “cup” and the “bowl.”

2.1 Acceleration Section

The acceleration system is a high-efficiency staged explosive launcher which relies on extensive momentum transfer between flyer plates to reduce the required mass. Depending on the materials used in the accelerator and the degree of optimization, the plates together are between 80-110 times the mass of the cup.

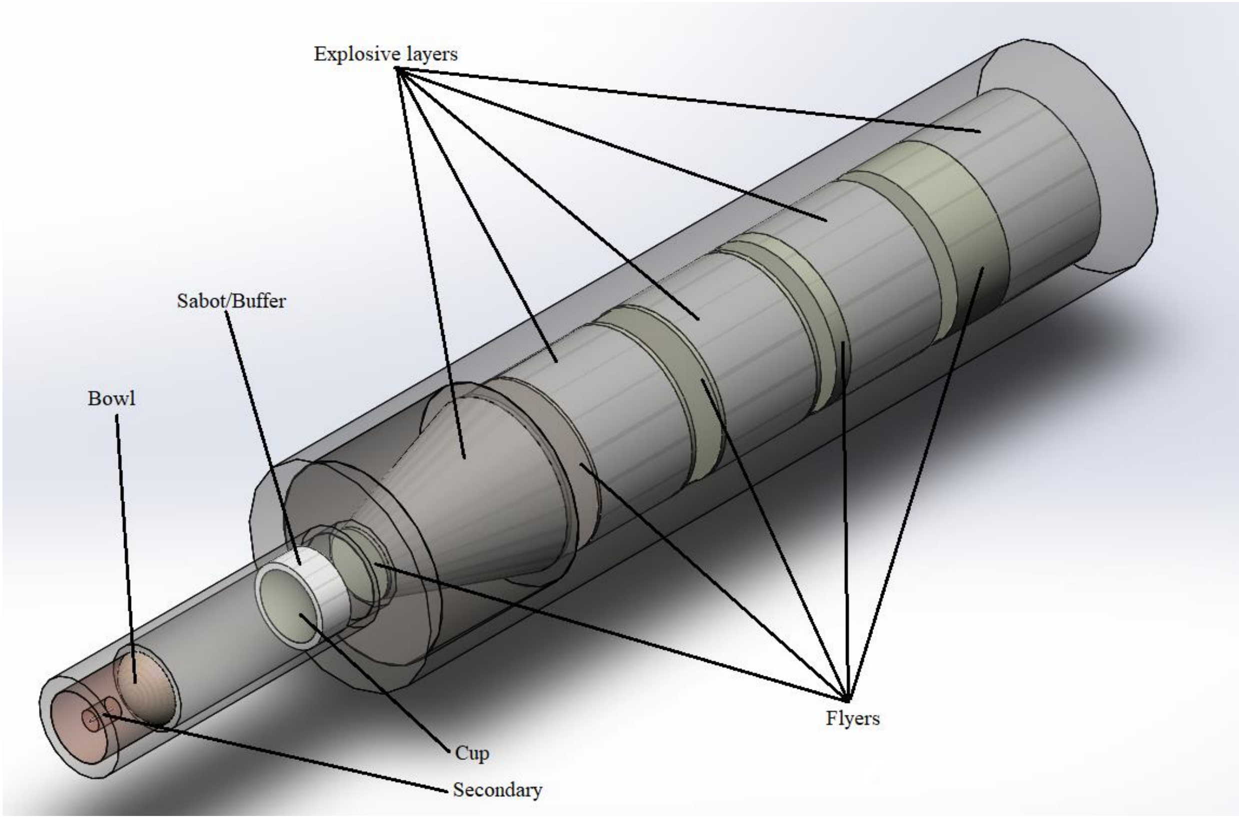

Figure 1: Model of the device

The simplified model of the device in Figure 1 shows the relative positions and sizes of the acceleration section and reaction section. The plates attached to the rear of the explosive layers in stages 3-5 act as tampers, delaying the rarefaction wave and smoothing irregularities in the compression wave.

2.2 Reaction Section

After combining the work of Winterberg, Ribe and Barnes, small changes were made to the reaction section so that it would be compatible with the acceleration section. In addition, the mechanism for transferring energy from the primary to the secondary was slightly changed from Winterberg's design. Winterberg uses a high-Z "diaphragm" between the stages which allows radiation and charged particles into the secondary hohlraum only after the energy release from the primary causes it to stretch and break. Here, the diaphragm is replaced with a low-Z material which maintains the plasma's inertial confinement while allowing radiation to pass. This improves the efficiency of the device because it allows energy to be transported to the secondary before the plasma in the primary has expanded.

2.3 Example Yields and Sizes

Because no fissile material is used, the theoretical lower yield boundary of the device is determined by the insulation time of the primary τ_E. Smaller primaries suffer from higher heat losses due to their larger surface area-to-volume ratio and will not undergo a complete reaction if they are sufficiently small. Barnes, Ribe and others did additional work to connect the final plasma properties with the initial properties of the impactors [5]. For a τ_E =1 μs, n=1E25 m^{-3}, T=6.5 KeV:

$$va > 20 \, {m^2}/{s}$$

$$v = impactor\ velocity$$

$$a = impactor\ radius$$

This corresponds to an impactor radius of 2 mm, a total length of 8 cm, a total diameter of 1.5 cm, a mass of 120 g and a yield of 2.5 kg TNT equivalent at the normal impact velocity of 10 km/s. However, extremely high precision would be required to manufacture this system. The real yield limit is probably on the order of 100 kg TNT equivalent.

The device in Figure 2 is on the low end of possible yields, with a mass of 20 kg, a length of 45 cm, a diameter of 8 cm and a yield of 250 kg of TNT. Scaled up to the largest reasonably portable size, the same design would have a mass of 1600 kg, a length of 2.5 m, a diameter of 40 cm and a yield of 2 kt of TNT.

The nonlinear relationship between mass and yield is primarily due to the differences in proportionality between the reaction section and the accelerator section. The yield of the secondary is proportional to the yield of the primary, which is in turn proportional to the volume enclosed by the cup. The mass of the accelerator is proportional to the mass of the cup, which is proportional to the product of the cup's area and thickness. However, the cup thickness is roughly constant because it is determined by the inertial confinement time, which is constant for all yields. So, the mass of the accelerator increases as the square of the cup radius, but the yield increases as the cube of the cup radius.

3.0 Theory

The operation of the system is intuitively simple, but impossible to model accurately without hydrodynamics code. The acceleration system in particular is a difficult nut to crack because of the paucity of data on explosive properties at high pressures.

3.1 Acceleration Section

Materials for flyer plates and explosive layers are both selected for maximum shock impedance, which enhances the pressure induced in the explosive layers. The pressure is calculated by finding the intersection point of the principal Hugoniot curve of the explosive layer material and the reflected Hugoniot curve of the flyer material. The graph in Figure 2 is a good depiction of the materials used in the accelerator. The target has a shallower Hugoniot curve than the impactor, indicating a lower shock impedance, which is the case for a tungsten impactor and an explosive target.

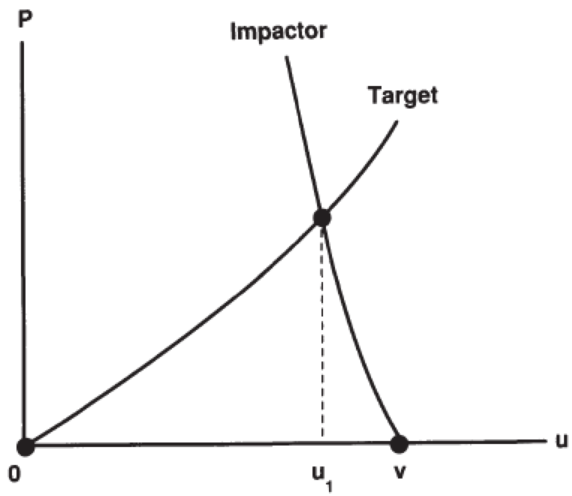

Figure 2: Determination of shock pressure from Hugoniot curves and impact velocity. From [6]

The final velocity of the flyer is determined by combining the velocity imparted to the flyer by the explosive layer and by the previous flyer. The velocity from the previous flyer is easy to calculate because both flyers are constructed from the same material. The impedance matching graph used to determine the shock pressure is flipped about itself so that the impactor Hugoniot is a principal Hugoniot and the resulting particle velocity is:

$$u = v - u_1$$

The flyer begins to move when the shock reaches its face and reflects a rarefaction wave backwards into the flyer. For reflection from a free surface, the particle velocity is:

$$u_{flyer} = 2 * u_1$$

The velocity imparted by the explosive is more difficult to determine because the explosive will undergo overdriven detonation at impact velocities above 3 km/s. This means that new physical properties for the explosive must be calculated before the Gurney equations can be used to find the velocity. Nobody really seems to agree on how this should be done analytically. A variety of different equations of state are listed in [7], including γ-law, Jones-Wilkins-Lee, and a few pet theories from several scientists (including the author).

I decided to select explosives based on the quantity of experimental data available, and do a power regression curve-fit with my TI-84. This is probably equal in accuracy (although inferior in intellectual rigor) to most of the equations of state. The resulting equation relates the volume compression ratio to the detonation pressure and is derived from the PBX-9404 data in [8] and [9]. The volume compression ratio is easily found from the particle velocity and physical properties of the explosive layer by using the equations in [6]:

$$\frac{V}{V_0} = \frac{C_0 + (S-1)u}{C_0 + Su}$$

$$P_{det} = 15.233 * \left(\frac{V}{V_0}\right)^{-3.072} \ (GPa)$$

The Gurney energy is found using the polytropic relations for an adiabatic process in ideal gases. The detonation pressure and volume compression ratio are used, with the assumption that the plate accelerates until the detonation products have expanded by a factor of two.

$$E_G = E_0 - E_v$$

$$E = \frac{Pv}{\gamma - 1}$$

$$P_{det} v_{det}^{\gamma} = P_f v_f^{\gamma}$$

$$v = \frac{V/V_0}{\rho_0}$$

$$E_G = \frac{P_{det} v_{det}}{\gamma - 1} - \frac{P_{det} \frac{v_{det}^{\gamma}}{v_f^{\gamma - 1}}}{\gamma - 1}$$

$$E_G = \frac{P_{det} v_{det}}{\gamma - 1} [1 - \left(\frac{v_{det}}{v_f}\right)^{\gamma - 1}$$

Since $v_f = 2v_{det}$ and $\gamma = 3$ for detonation products,

$$E_G = \frac{3}{8} P_{det} v_{det}$$

$$V_G = \sqrt{\frac{3}{4} P_{det} v_{det}}$$

The velocity imparted by the explosive is then found by using the Gurney relation for asymmetrical explosive sandwiches:

$$u_{flyer} = V_G \left(\frac{1 + A^3}{3(1 + A)} + A^2 \frac{N}{C} + \frac{M}{C}\right)^{-1/2}$$

$$A = \frac{1 + 2\frac{M}{C}}{1 + 2\frac{N}{C}}$$

Where C is the explosive mass, N is the tamper mass and M is the flyer mass. The flyer velocities are then added to find the final velocity, which is a gross oversimplification of the real situation. In reality, the explosive and flyer will not be at rest with respect to each other prior to detonation because they have different shock impedances and therefore different particle velocities. This invalidates the Gurney relations, but I'm using them anyways because the alternatives are many times more complicated.

When the flyer collides with the explosive layer, a compression wave travels through the explosive and the flyer. When the compression wave reaches the rear of the flyer, the pressure is released and a rarefaction wave begins travelling back towards the explosive layer. Because the rarefaction wave is faster than the compression wave, it will eventually catch up to the compression wave and return the detonation to ordinary CJ conditions. This is prevented by using a sufficiently thick impactor and tamper.

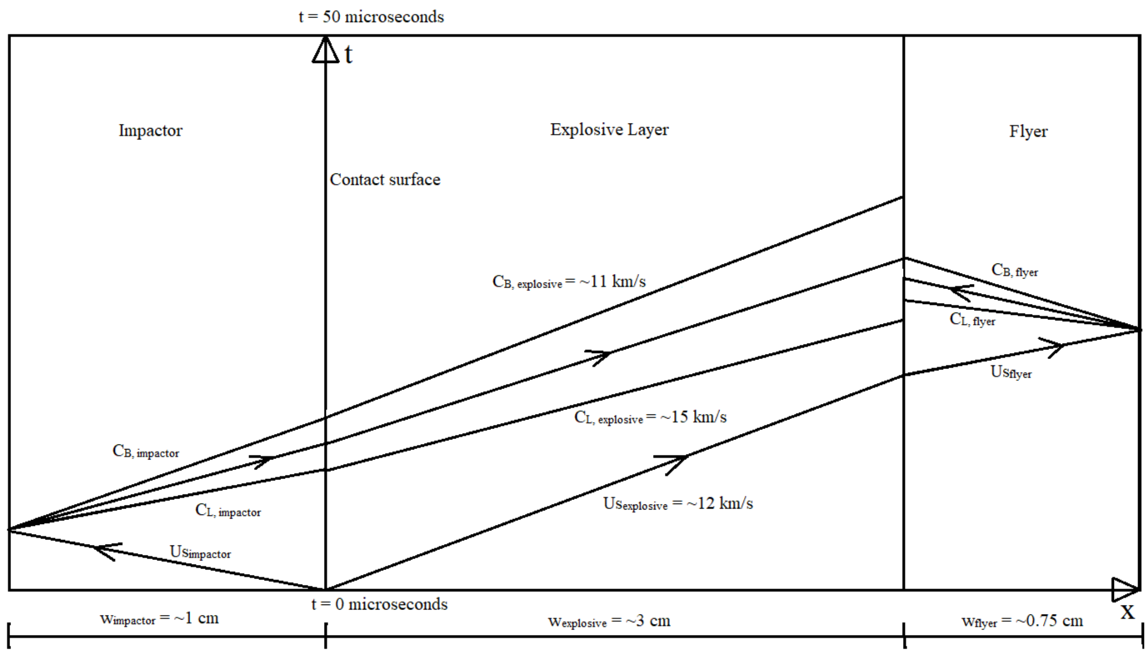

Figure 3: Lagrangian time-distance diagram of the shock transmission process

The ideal case where the main rarefaction wave does not intercept the compression wave is shown in Figure 3. Rarefaction waves are split into "fans" because of the pressure dependency of the bulk and longitudinal sound speed, which causes the wave to stretch as it travels. To prevent spallation, the main rarefaction wave should intersect the flyer rarefaction wave at the interface between the flyer and the explosive. The tamper is omitted for clarity, but it would be placed between the impactor and the explosive layer. Representative values for the shock and rarefaction wave velocities in the fourth or fifth stage are shown. Appropriate thicknesses for the impactor, tamper, layer and flyer can be found by equating the travel times of the rarefaction waves so that they meet between the explosive and the flyer.

$$t = \frac{w_{exp}}{U_{exp}} + \frac{w_{flyer}}{U_{flyer}} + \frac{w_{flyer}(V/V_0)_{flyer}}{C_{L,flyer}}$$

$$t = \frac{w_{imp}}{U_{imp}} + \frac{w_{imp}(V/V_0)_{imp}}{C_{L,imp}} + \frac{w_{exp}(V/V_0)_{exp}}{C_{L,exp}}$$

Imperfections on the surface of the flyer plates must be minimized to increase the durability of the plates. Bat'kov notes in [3] that plates must ideally have thickness gradients of less than 0.1%.

Explosive layers with a sufficiently high aspect ratio should have side containment constructed out of a high-Z material to reduce side rarefaction losses. This can be seen in the model depicted in Figure 1, which has a thick casing to contain the explosive until each flyer has been fully accelerated.

The last stage(s) should use conical tunnels [10] to enhance shock pressures and velocities via convergence. This also allows a thicker plate to be used for the same mass ratio between flyers, since the surface area of the flyer is decreased.

The flyer which impacts the rear of the "cup" should have a graded-density buffer. Graded-density buffers use layers of materials with progressively higher shock impedances to prolong the duration of a shock via interreflection [11]. This reduces the magnitude of the peak pressure on the "cup" and allows it to maintain its shape during acceleration, which is critical to the performance of the reaction section.

Without some method of transferring kinetic energy from a low-velocity (<2 km/s) flyer to the next stage before it contacts the explosive layer, the energy transfer efficiency will be impacted because the explosive will detonate and expand before the shock can travel through it.

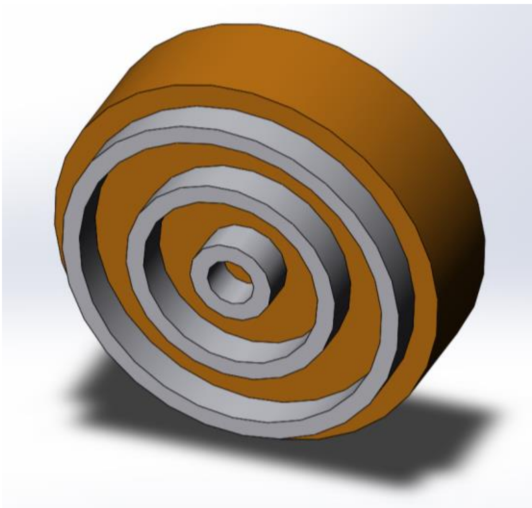

Figure 4: Potential spacer arrangement

One possible method of transferring kinetic energy is depicted in Figure 4. Concentric rings of material with a high bulk sound speed are embedded in the explosive layer, and transmit a shock into the next flyer.

3.2 Reaction Section

After the cup begins to move, the design is identical to the one proposed by Ribe & Barnes, and the theoretical equations used are the same. The "cup" travels down a tube which is surrounded by helical conductors and filled with DT gas. The interior dimensions of the cup and the tube, as well as the initial DT gas pressure, are determined by the desired final number density of the plasma [12].

$$\rho_0 = \frac{n * N_A}{M_{DT}} \frac{V_0}{V}$$

$$P_0 = \rho_0 RT$$

The magnetic insulation time τ_E is calculated for a variety of conditions in [13]. This paper was written by researchers at the Science Applications International Corporation (SAIC), so I was only able to find the version of the equation used in [2]. This is for a characteristic magnetic field of B=200 T and T_f=10 keV.

$$\tau_E = 3.8E9 * \Delta f^2 / n^{0.4}$$

The thickness of the cup is determined by the desired inertial confinement time, which must be roughly equal to the magnetic insulation time. From [2]:

$$\tau_b = \left\{ \left[\left(1 + \frac{\Gamma}{2}\right) (1 + x)^3 - \frac{2}{\Gamma} \right]^{\frac{1}{2}} - 1 \right\} * \Delta f / u_s$$

Where Γ is the Gruneisen coefficient of the shell material, Δf is the final radius of the plasma cavity, x is the ratio between the final shell thickness and Δf and u_s is the velocity of the stopping shock which travels outwards from the plasma cavity when the maximum compression ratio is reached. The shock velocity is determined from the final pressure in the shell, which is calculated from the final temperature and ion number density:

$$P_f = 2nT_f$$

For a tungsten shell and an assumed final temperature prior to the thermonuclear burn of T_f = 10 KeV, the equation becomes:

$$\tau_b = 1.7E9 * \left\{ [2(1 + x)^3 - 1]^{\frac{1}{2}} - 1 \right\} * \frac{\Delta f}{n^{1/2}}$$

The calculations for the helicity injection system are complicated by the network of interdependencies between it and the other components. Once specifications for the rest of the device have been determined, the system is designed using [12] as a guide. Figure

5 shows the simplified model used to calculate the behavior of the injection system. In reality, the conductors are closely spaced and the piston is considerably thinner.

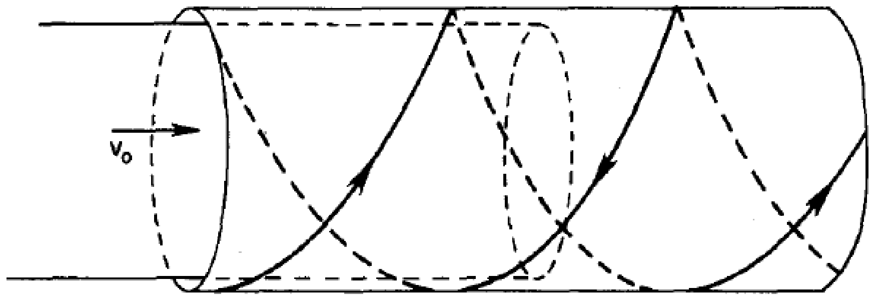

Figure 5:Model of helicity injection system showing piston, cylinder and conductors. From [12]

$$\dot{H}_R = Time\ derivative\ of\ relative\ helicity$$

$$B_0 = Initial\ magnetic\ field\ strength$$

$$a = cylinder\ radius$$

$$v_0 = initial\ piston\ velocity$$

$$\Delta = piston\ thickness$$

$$\delta = normalized\ piston\ thickness\ \frac{\Delta}{a}$$

$$\kappa = conductor\ winding\ pitch$$

$$d = csch\delta$$

$$f = \frac{\kappa - dsin\kappa\delta}{1 + \kappa^2}$$

$$\dot{H}_R = -2\pi a^3 v_0 B_0^2 f$$

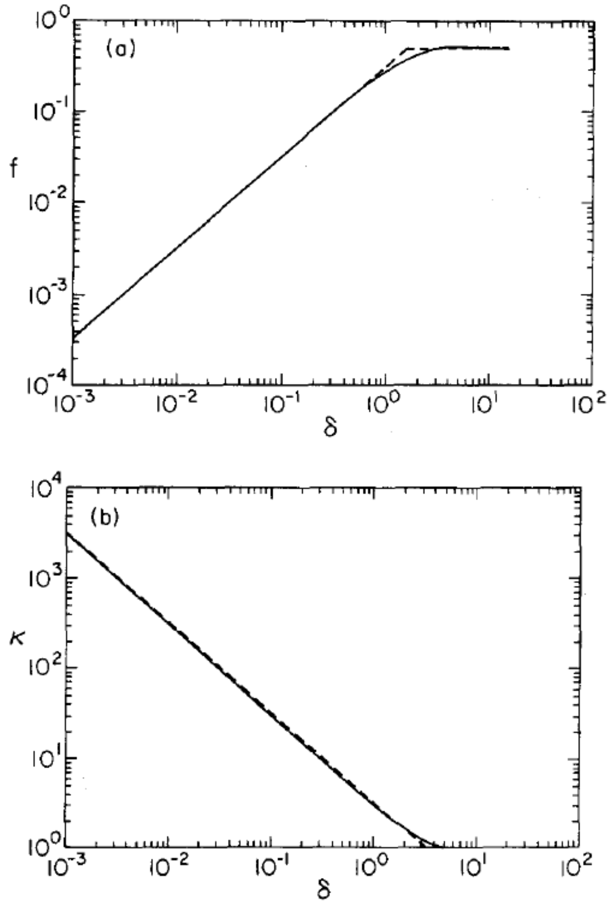

Figure 6: κ and f as a function of δ. From [12]

δ is fixed at approximately ~0.15 for this design due to constraints imposed by the other components. Therefore, the winding pitch κ is fixed at ~20 and the helicity injection rate $\dot{H}_R$ is proportional to the cube of the cylinder radius multiplied by the square of the initial field strength.

One aspect of hypervelocity engineering which is missing from Ribe & Barnes' design is avoiding metal-on-metal contact. At speeds of 10 km/s, any sliding contact between metals causes forces that drastically exceed the yield strength of the material. The resulting carnage is visually similar to the effect produced by rubbing ripe bananas together. This can be avoided by surrounding the cup with a polymer sabot containing embedded conductors.

As the cup travels down the tube, it initiates a shock in the DT gas, which compresses and heats the gas ahead of the cup. Because the cup and bowl have a much higher shock impedance than the DT gas, the shock is reflected between them multiple times as they move closer. This process rapidly heats and compresses the DT gas until it becomes a plasma. The pressure and temperature increase for each shock can be found with the Rankine-Hugoniot jump conditions for strong shocks in ideal gases.

$$C = \sqrt{kRT}$$

$$\frac{p_2}{p_1} = (\frac{u_p}{C})^2 \frac{\gamma(\gamma + 1)}{2}$$

$$\frac{T_2}{T_1} = \frac{\gamma - 1}{\gamma + 1} \frac{p_2}{p_1}$$

The particle velocity u_p is equal to the velocity of the cup. Since C increases with temperature, the term $(\frac{u_p}{C})^2$ approaches a minimum and the temperature of the gas approaches a maximum. For DT gas and a cup velocity of 10 km/s, these values are 1.83 and ~9500 K. The pressure of the gas continues to increase by a factor of four with the passage of each shock.

Once the cup contacts the bowl, it undergoes a quasispherical implosion which is caused by the geometry of the cup. This, along with the magnetic insulation of the plasma, is essential to reducing the impact velocity requirements [2]. Spherical implosions are the most efficient variety of implosion available in three dimensions, since the volume of the cavity is reduced at a rate proportional to the cube of the implosion velocity [14], [15].

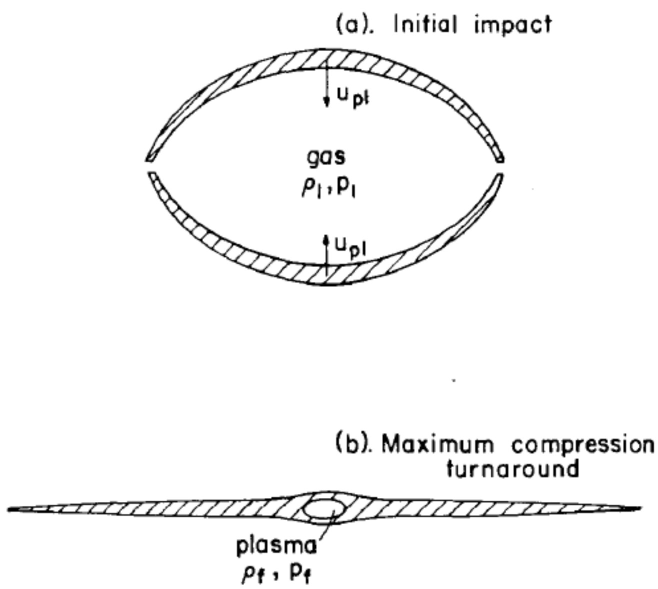

Figure 7: Quasispherical implosion of a shaped metallic shell. From [2]

The quasispherical implosion increases the density of the magnetic field and the DT plasma. All of the designs I worked out used a compression ratio of V_0/V=1000 and a final ion number density of 3E28 m^{-3} to ensure an efficient burn. The thermonuclear energy release W_{TN} is given by:

$$W_{TN} = 3.24E^{-34} * n^2 * \Delta f^3 * \tau_b$$

This results in a large neutron and alpha-particle release. The neutrons are assumed to escape because the cup and bowl are constructed out of a high-Z material and are not highly compressed. At this point, the system diverges from Ribe & Barnes' design and begins to make use of Winterberg's ideas.

Rayleigh-Taylor instabilities will be rapidly established on the internal surfaces of the cup and bowl either through natural processes or by deliberately machining seeding surfaces on the walls. The reason for the introduction of R-T instabilities is increase the production of blackbody radiation through heat conduction from the plasma to the wall material. This radiation is used for the same purpose as in a conventional thermonuclear device-to implode a Li^6D secondary stage. The temperature of the radiation is found with the Stefan-Boltzmann Law, assuming that the radiation fills the space occupied by the primary and secondary hohlraum and achieves equilibrium.

First, the volumetric energy density of the plasma is found. This assumes that the neutron energy is entirely lost to the plasma and the α-particles are entirely contained:

$$e_\alpha(erg/cm^3) = \frac{0.2 * W_{TN} * 1E7\ erg/J}{V\ (cm^3)}$$

Then the temperature:

$$T = \sqrt[4]{\frac{e_\alpha * c\ (cm/s)}{4 * 5.669E - 5}}\ (K)$$

The efficiency of the primary corresponds to the temperature of the radiation. Generally, this should be in the soft X-Ray region of the electromagnetic spectrum between 0.8-1 keV. The wall of the bowl between the primary and secondary is an X-Ray window constructed out of Be, B, Li, or LiD. The window also serves to reduce neutron flux from the primary-excessive neutron heating in the secondary would cause inefficient compression and could lead to a fizzle. Radiation from the primary passes through this window and begins to ablate the surface of the secondary tamper.

An important check on the relative sizes of the secondary and primary is the energy required to implode the secondary. Using simple Newtonian equations, for a cylindrical secondary:

$$W = Fd = PAd$$

$$W = 2\pi PL \int_{r_0}^{r_f} rdr$$

$$W = \pi PL({r_0}^2 - {r_f}^2)$$

Based on (FIND THIS ICF SOURCE), the pressure P is:

$$P\ (Pa) = 3E4 * T^{\ 3.5}(eV)$$

To find the conditions existing in the secondary at the end of compression, it is necessary to calculate the behavior of the tamper. The tamper can be modeled as an inverted rocket, and the Tsiolkovsky rocket equation is used to find its final implosion velocity assuming that ¾ of the tamper mass is lost to ablation:

$$V_e = 1E6 * T^{\frac{1}{2}}\,(cm/s)$$

$$V_{imp} = V_e Ln(4)$$

The final compression pressure is the pressure exerted by the ablation of the tamper, which is found above. The compression ratio resulting from that pressure can be assumed to be the adiabatic limit of an infinite number of shocks. This is because the secondary has a very small radius, which allows shocks to traverse it multiple times during the compression process. The compression is split into the final compression $R_{c,f}$ and the initial compression $R_{c,i}$ which is caused by the initial ablation shock propagating through the secondary. This shock is assumed to have an amplitude of 50 Mbar.

$$R = \left(\frac{P}{P_0}\right)^{\gamma}$$

$$\rho_f = R_{c,f} * R_{c,i} * \rho_i$$

This makes it possible to find the number density and mean free path of the resulting compressed material. A 14.1 MeV neutron MFP which is smaller than the radius of the compressed secondary ensures that the secondary undergoes an efficient reaction. The initial MFP for Li^6D is 10.8 cm [16].

$$n = \frac{\rho N_A}{M}$$

$$Mean\ free\ path = \frac{(MFP)_i}{R_{c,f} R_{c,i}}$$

This results in a cylindrical implosion with similar conditions to the ICF experiments performed at the National Ignition Facility, but with a much larger quantity of fuel. The small diameter of the secondary and the relatively long confinement time of the primary allows for a “spark-initiated” fusion burn. Spark-initiated burns rely on shock convergence to produce extremely high temperature and pressure in the central region of a cylindrical or spherical pellet of fusile material. Once fusion begins in the center, it propagates outwards before the pellet can be disassembled. As in a conventional thermonuclear device, the secondary increases the yield by a factor of 10-100.

4.0 Proliferation Concerns

The potential impact of pure-fusion nuclear devices on the current regulatory framework has been studied in the past [17]. Non-proliferation efforts worldwide rely entirely on the stringent manufacturing constraints of fission primaries. Because this design does not require explosive lenses, isotope enrichment or high-precision machining, it strongly increases the likelihood that non-state actors will acquire thermonuclear weapons.

In order of increasing difficulty, the operations required to complete a rudimentary version of this device are: machining the accelerator casing and plates; machining the reaction section components; filling the reaction section with DT gas; laying the helical windings on the reaction section casing; and producing/machining the explosive layers.

The primary bottlenecks for an organization of limited resources are the production of tritium and high-quality plastic-bonded explosives.

5.0 Applications

The military applications of a highly scalable thermonuclear explosive are obvious. One interesting aspect of the design is the wildly diverging degree of neutron shielding provided by different sections of the device. Neutrons travelling “up” towards the remnants of the accelerator will be heavily impeded by the layers of pressurized low-Z detonation products. They will surrender most of their kinetic energy to the products, resulting in an intense blast of plasma.

Under ordinary conditions, the tamper is extremely inefficient at neutron moderation. However, the compression process will increase the number density of the tamper by several hundredfold, ensuring that neutrons will be forced to collide with hundreds of atoms before escaping. Neutrons travelling perpendicular to the wall of the secondary will be thermalized by the intensely compressed tamper. The tamper will be heated by neutrons, alpha particles and bremsstrahlung until it emits gamma rays, but will remain at high density due to the extreme pressures until a rarefaction wave arrives. At this point, the tamper will vaporize and a wave of ionizing radiation, neutrons and plasma will be released into the exterior casing.

Finally, since the “bottom” of the device consists of a thin layer of uncompressed high-Z material, neutrons which are headed “down” will sail through unimpeded. This will create a cone of high-energy neutrons. The lethal range of that cone is approximated by the graph in Figure 8.

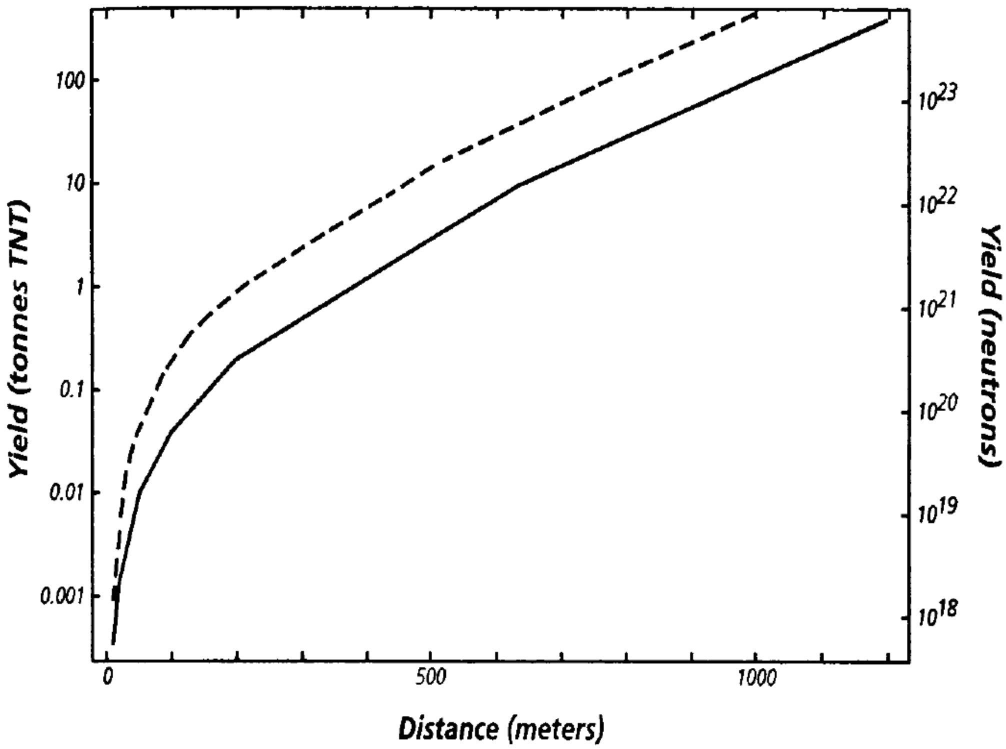

Figure 8: Lethal (4.5 Gy) radius of a 14 MeV neutron point source in open (solid) and built-up (dashed) areas. From [17]

The primary non-military application of pure-fusion explosives would be in space propulsion. Nuclear pulse propulsion, in general, provides extremely high thrust and specific impulse. The high energy densities available in thermonuclear explosives could be exploited without fallout concerns. The layered plates and detonation products produced by the accelerator section would slow the DT neutrons down to the fission spectrum, eliminating the requirement for radiators and harnessing the large proportion of DT fusion energy which is released in the form of neutrons. The pulse units are significantly denser than conventional propellants and require no cryogenic storage. Finally, the pulse units are primarily constructed out of cylindrical blocks of metal. With only a rudimentary ability to refine and machine asteroidal material, large cost savings could be accomplished by boosting into orbit only the fusile material and explosive layers.

References

[1] F. Winterberg, "Magnetic Booster Target Low Velocity High Yield Impact Fusion," *IEEE Transactions on Magnetics,* vol. 18, no. 1, pp. 213-216, 1982.

[2] F. Ribe and D. Barnes, "Review of Impact Fusion Targets," *IEEE Transactions on Magnetics,* vol. 25, no. 1, pp. 20-26, 1989.

[3] Y. V. Bat'kov, N. P. Kovalev, A. D. Kovtun, V. G. Kuropatkin, A. I. Lebedev, Y. M. Makarov, S. F. Manachkin, S. A. Novikov, V. A. Raevsky and Y. M. Styazhkin, "Explosive Three-Stage Launcher to Accelerate Plates to Velocities more than 10 km/s," *International Journal of Impact Engineering,* vol. 20, pp. 89-92, 1997.

[4] A. Geille, "Status of Development of Space-Debris Hypervelocity Multi-Stage Launcher," *International Journal of Impact Engineering,* vol. 20, pp. 271-279, 1997.

[5] D. Barnes, R. Bishop, G. Bourianoff, G. Craddock, W. Nystrom and F. Ribe, "Compact Magnetically Insulated Impact Fusion (MIIF) System," in *Bulletin of the American Physical Society*, New York, 1988.

[6] J. R. Asay and M. Shahinpoor, High-Pressure Shock Compression of Solids, New York: Springer Science+Business Media, 1993.

[7] Z.-Y. Liu, "Overdriven Detonation Phenomenon and its Applications to Ultra-High Pressure Generation," Kumamoto University, 2001.

[8] J. Kineke and C. West, "Shocked States of Four Overdriven Explosives," in *Fifth Symposium (International) on Detonation*, Pasadena, 1970.

[9] E. Lee, M. Van Theil, L. Green and A. Mitchell, "Detonation Product EOS: The Region Above Chapman-Jouguet Pressure," in *Shock Waves in Condensed Matter*, Santa Fe, 1983.

[10] Z.-Y. Liu, S. Kubota and S. Itoh, "Numerical Study on Hypervelocity Acceleration of Flyer Plates by Overdriven Detonation of High Explosive," *International Journal of Impact Engineering,* vol. 26, pp. 443-452, 2001.

[11] L. Chhabildas, J. Dunn, W. Reinhart and J. Miller, "An Impact Technique to Accelerate Flier Plates to Over 12 km/s," *International Journal of Impact Engineering,* vol. 14, pp. 121-132, 1993.

[12] D. Barnes, "Mechanical Injection of Magnetic Helicity," *The Physics of Fluids,* vol. 31, no. 8, pp. 2214-2220, 1988.

[13] D. Barnes, F. Ribe, G. Bourianoff, J. McBride, D. Schnack and G. Craddock, "Magnetically Insulated Impact Fusion (MIIF)," in *Bulletin of the American Physical Society*, New York, 1987.

[14] R. M. Zubrin and F. L. Ribe, "Numerical Studies of Deuterium-Tritium Ignition in Impact-Fusion Targets," *IEEE Transactions of Plasma Science,* vol. 17, no. 3, pp. 459-462, 1989.

[15] L. Sankaran, "Numerical Studies of Impact-Fusion Target Dynamics," University of Washington, 1987.

[16] A. Hemmendinger, C. Ragan, E. Shunk, A. Ellis, J. Anaya and J. M. Wallace, "Tritium Production in a Sphere of LiD Irradiated by 14 Mev Neutrons," Los Alamos National Laboratory, Los Alamos, 1978.

[17] S. L. Jones and F. N. von Hippel, "The Question of Pure Fusion Explosives Under the CTBT," *Science & Global Security,* vol. 7, pp. 129-150, 1998.